DIRECT NUMERICAL SIMULATION OF OBLIQUE VORTEX SHEDDING FROM A CYLINDER IN SHEAR FLOW

Jorge H. Silvestrini
Departamento de Engenharia Mecânica e Mecatrônica,
Faculdade de Engenharia,
Pontifícia Universidade Católica do Rio Grande do Sul
Av. Ipiranga 6681, 90619-900 Porto Alegre - RS, Brasil
jorgehs@em.pucrs.br

Eric Lamballais
Laboratoire d'Etudes Aérodynamiques UMR 6609,
Université de Poitiers,
Téléport 2 - Bd. Marie et Pierre Curie B.P. 30179
86962 Futuroscope Chasseneuil Cedex, France
lamballais@univ-poitiers.fr

ABSTRACT

The vortex dynamics of a shear flow over a circular cylinder is studied by means of Direct Numerical Simulation. A numerical code based on Cartesian grids and accurate schemes is used in combination with an immersed boundary method. The flow configurations are selected in order to consider the influence of three physical parameters: the vertical extension of the shear zone, the vertical domain size and the shear intensity. Different combinations of these three parameters are considered by maintaining constant the median Reynolds number. For each case, the non-uniform character of the upstream flow leads to the formation of complex Kármán streets behind the cylinder. The analysis of the animations shows the occurrence of oblique vortex shedding driven through complex synchronization processes. The shear imposes strong distortions on the Kármán vortices and dislocations are currently observed. Depending on the local Reynolds number (associated to the inflow velocity profile), highly three-dimensional secondary structures are observed in the high-speed region of the flow. The simple observation of the animations does not allow a unambiguous identification of the cellular pattern of vortex shedding. This phenomenon can be more rigorously described by a frequency analysis presented in this paper. It is shown that the main frequency selection is mainly conditioned by a local adjustment of oblique vortex shedding on the upstream velocity. However, due to the preservation of the spatial coherence of the flow, the variation of the main flow frequency occurs by jump along the cylinder axis direction, the distance between two jumps corresponding to the size of a cell. The Kármán vortex formation is triggered in the high-speed region of the flow, but paradoxically, the local vortex shedding frequency found in this zone seems to be strongly influenced by the dynamics of the slow part of the flow.

INTRODUCTION

Oblique vortex shedding is a common feature in many engineering applications such as marine risers, pillars of offshore platforms and bridges, heat exchangers or ultra-clean protection devices in food industry. In this last case, a recent research on the interactions between a mixing layer and a wake shows the important link between oblique vortex shedding and mean vertical currents behind a circular cylinder oriented in the shear direction associated to the mixing layer (Heitz, 1999; Lamballais and Silvestrini, 2002). These interactions impose a strong asymmetry in the vertical (i.e. parallel to the cylinder axis) organization of the wake. Two dynamically different zones have been clearly identified in these experimental (Heitz, 1999) and numerical (Lamballais and Silvestrini, 2002) studies: a low-speed wake which follows the behaviour of a conventional wake (produced by a uniform flow) and a high-speed wake that is largely influenced by the vertical currents and highly three-dimensional. Following the main objective of understanding the oblique vortex shedding phenomena, this paper presents numerical results of a shear flow over a circular cylinder. Contrary to these previous studies, where the shear region of the upstream flow was spatially compact (the mixing layer thickness was close to the cylinder diameter), we consider here a flow geometry where the vertical extension of the constant shear zone is at least one order magnitude larger than the cylinder diameter. In this flow configuration, the spatial repartition of the shear effects on the vertical organization of the motions occurs *a priori* more gradually, in such a way that the links between the main three-dimensional phenomena (non-parallel vortex shedding, secondary vortex creation) should be easier to establish.

For this type of flow, where the cylinder axis is perpendicular to the upstream flow velocity and vorticity vectors at the same time, interesting results was reported in previous experimental (Maull and Young, 1973; Stansby, 1976; Tavoularis et al., 1987, Woo et al. 1989), numerical (Mukhopadhyay et al., 2002) and theoretical (Noack et al., 1991) studies. The complex nature of this flow geometry was clearly shown through the identification of numerous physical processes related to a specific vortex dynamics where oblique vortex shedding, dislocations and cell formations are the main ingredients. The understanding of these phenomena and their eventual links needs to be improved, especially for practical applications where a fluid control strategy is required. The goal of this study is to examine these mechanisms by taking advantage of the full information offered

by Direct Numerical Simulation (DNS). The use of a high spatial resolution allows us to consider flow regimes where three-dimensional motions play an important role with and without the presence of a shear on the upstream flow. This is in contrast to the previous numerical study of Mukhopadhyay et al. (2002) where the Reynolds numbers considered lead to a nominally two-dimensional dynamics when a uniform inflow is imposed.

The paper is organized as follows. After the introduction of the flow configuration, some details about the numerical methods are shortly presented. Then, instantaneous visualizations of the vortical organization of each simulated flow are shown and analysed. In a second step, quantitative results are presented through a frequency analysis in order to better understand the physical mechanisms responsible of the local selection of vortex shedding processes.

FLOW CONFIGURATION AND PARAMETERS

A shear flow over a circular cylinder of diameter D is considered in a Cartesian frame of reference $\mathcal{R} = (0; x, y, z)$. The cylinder axis is oriented along the vertical direction y at the intersection between the streamwise section x_{cyl} and the spanwise one $z = 0$ (see figure 1). At the inflow section, the constant shear is aligned in the y-direction and extended in a zone $-L'_y/2 < y < L'_y/2$. Outside this interval, two streams of constant velocities U_1 (for $y < -L'_y/2$) and U_2 (for $y > L'_y/2$) are imposed, with by convention $U_1 > U_2$. The inflow velocity profile $U(y)$ at $x = 0$ is given by

$$U(y) = \frac{U_1 + U_2}{2} + \frac{U_2 - U_1}{12}\frac{D}{L'_y}\left\{\ln\left(\frac{\cosh[\frac{6}{D}(y + \frac{L'_y}{2})]}{\cosh[\frac{6}{D}(y - \frac{L'_y}{2})]}\right)\right\} \quad (1)$$

without any additional perturbations (steady inflow condition). This shape of profile allows us to consider a constant shear flow extending on a wide region while preserving the free-slip conditions imposed at $y = \pm L_y/2$. Note that contrary to the generic case of a cylinder wake due to a uniform upstream flow, the present flow configuration prevents to consider an infinitely long cylinder (well represented by the use of a periodic condition) due to the necessarily limited extent of the shear region of the upstream flow. The presence of free-slip walls, equivalent to mirror conditions assumed at $y = \pm L_y/2$, impose a kinematic blocking associated to the condition $u_y(x, \pm L_y/2, z) = 0$. As a first consequence, this condition breaks the homogenous character of the mean flow in y-direction. For the conventional case of a wake due to a uniform flow, Lamballais and Silvestrini (2002) have shown that the main features of the wake dynamics was preserved when free-slip walls were used instead of periodic boundary conditions, especially concerning the vortex shedding which was found to be parallel for both cases. In this sense, the oblique mode selection found in this work can be viewed as an intrinsic feature of the flow under study rather than a secondary consequence of the set of boundary conditions used in y-direction. Moreover, by choosing the condition $L_y \gg L'_y$, it is possible to reduce the blocking effect while distinguishing three basic flows in the computational domain: a high-speed wake ($-L_y/2 < y < -L'_y/2$), a skewed-wake ($-L'_y/2 < y < L'_y/2$) and a low-speed wake ($L'_y/2 < y < L_y/2$). Note finally that a periodic boundary condition is imposed in z-direction.

DNS of a shear flow over a circular cylinder was performed by considering two shear parameters $\beta = 0.1, 0.025$

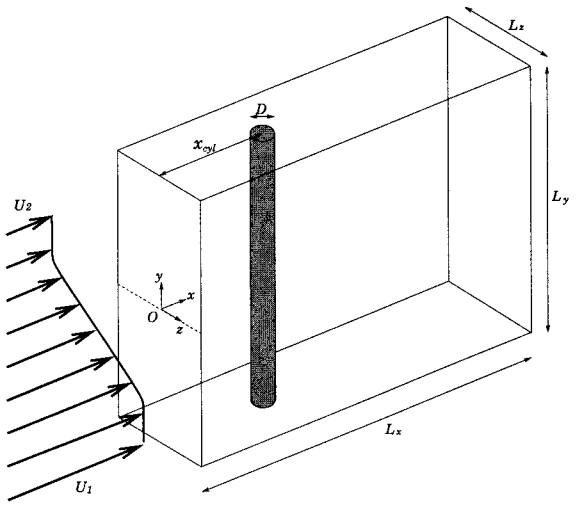

Figure 1: Schematic view of the flow configuration.

defined by

$$\beta = -\frac{D}{U_c}\frac{dU}{dy} \quad (2)$$

where $U_c = (U_1 + U_2)/2$ is the median velocity. Note that both couples of parameters (β, L'_y) considered here yields to $U_1 = 3U_c/2$ and $U_2 = U_c/2$. The corresponding Reynolds number ($Re = U_c D/\nu$) is 200, the local Reynolds number associated to the inflow velocity profile (1) varying from $Re_1 = U_1 D/\nu = 100$ to $Re_2 = U_2 D/\nu = 300$. For all calculations presented in this paper, the cylinder is located at $x_{cyl} = 7D$.

In what follows, four DNS are presented (see table 1). For three calculations, a different vertical dimension of the domain L_y is used while maintaining constant the extension of the constant shear zone $L'_y = 10D$. The comparison between these three cases allows us to examine the effects of the flow conditions in the neighbourhood of the shear region limits $y = \pm L'_y/2$, where free-slip walls (case OW1) or low- and high-speed wakes (cases OW2 and OW3) can be present. In the fourth case OW4, the shear intensity is moderate with a shear zone extended to $L'_y = 40D$.

NUMERICAL METHODOLOGY

The incompressible Navier-Stokes equations are directly solved on a computational grid of $n_x \times n_y \times n_z$ points in non-staggered configuration. Sixth-order compact centred difference schemes are used to evaluate all spatial derivatives, except near the in- and outflow boundaries where single sided schemes are employed for the x-derivative calculation. Time integration is performed with a third-order low-storage Runge-Kutta method. For more details about the numerical code, see Lardeau et al. (2002) and Silvestrini and Lamballais (2002).

Despite its fundamental character, the flow geometry considered in this study presents some difficulties linked to the requirements of DNS in terms of accuracy and computational cost. Near the body, a cylindrical grid is *a priori* well suited, but further downstream in the flow, the increase of azimuthal mesh sides associated to this type of grid organization is a drawback. In order to avoid the difficulties associated to more sophisticated grids (loss of accuracy associated to mesh distortions, increase of the computational cost, ambiguity associated to the definition of an optimal grid), we use here an "immersed boundary method". More precisely, the presence of the cylinder is modelled with the aid of a

Table 1: Flow configurations and simulation parameters.

Case	(L_x, L_y, L_z)	(n_x, n_y, n_z)	L'_y	β
OW1	$(22D, 12D, 12D)$	(397,97,216)	$10D$	0.1
OW2	$(22D, 24D, 12D)$	(397,193,216)	$10D$	0.1
OW3	$(22D, 48D, 12D)$	(397,385,216)	$10D$	0.1
OW4	$(22D, 48D, 12D)$	(397,385,216)	$40D$	0.025

feedback forcing (Goldstein et al. 1993) that "freezes" the fluid in the body region. In a previous study (Lamballais and Silvestrini, 2002), we have shown that this method can be combined with a code based on high-order finite difference schemes for producing reliable results in the case of a conventional cylinder wake, especially for the prediction of the Strouhal number, the mean velocities, the turbulent stresses or the vortical organization of the flow. Here, we use the same numerical methodology with similar spatial and temporal resolutions (by taking the Reynolds number into account), in such a way that equivalent accuracy can be expected for the present results (see table 1 for additional details on simulation parameters).

RESULTS

General view of the flows

Figure 2 shows perspective views of the vorticity modulus divided locally by the inlet streamwise velocity given by (1). Using this normalization, it is possible to avoid the lack of vortical structure identification in the slow region of the flow where the level of vorticity is obviously weaker than in the fast region. By this method, a well-balanced view of the structural organization of the flow can be obtained. These pictures were taken at the final time of each calculation. The animations[1] are presented for a temporal sequence of $T = 78D/U_c$. Note that all results presented in this paper were obtained after the transient time for which statistically steady conditions are established. The views presented on figure 2 illustrate very well the complexity of this type of flow. In all cases, oblique Kármán vortices can be observed behind the cylinder. At this preliminary stage of the flow analysis, it is useful to notice that the oblique organization of the Kármán vortices arises from two cumulative effects.

The primary origin of the oblique structure is related to the slantwise vortex shedding itself. It is well known that non-parallel vortex shedding can occur even if upstream conditions correspond to a uniform flow in an extended region. In particular, it was shown clearly that end conditions for a finite cylinder are able to determine the vortex shedding mode (parallel/oblique selection, see Williamson, 1996 and Mittal, 2001). In the present flow configuration, the oblique vortex shedding is obviously related to the presence of the upstream shear. However, it is worth noting that the extent of regions where oblique vortex shedding is found do not correspond necessarily to a shear region. Hence, the preservation of oblique vortex shedding in the subdomain $y \in [-L_y/2, -L'_y/2]$ is not *a priori* expected for the case OW3 since in this region, the upstream flow is constant over a large y-extension of $L_y/2 - L'_y/2 = 19D$. In contrast, the return to a conventional two-dimensional vortex shedding can be clearly observed in the low-speed region of the OW3 flow, as shown by the view 2(c). The analysis of animations illustrates very well the physical mechanisms associated to

[1] Animations (mpeg format) are available on the internet link http://labo.univ-poitiers.fr/informations-lea/tsfp3paper/index.htm

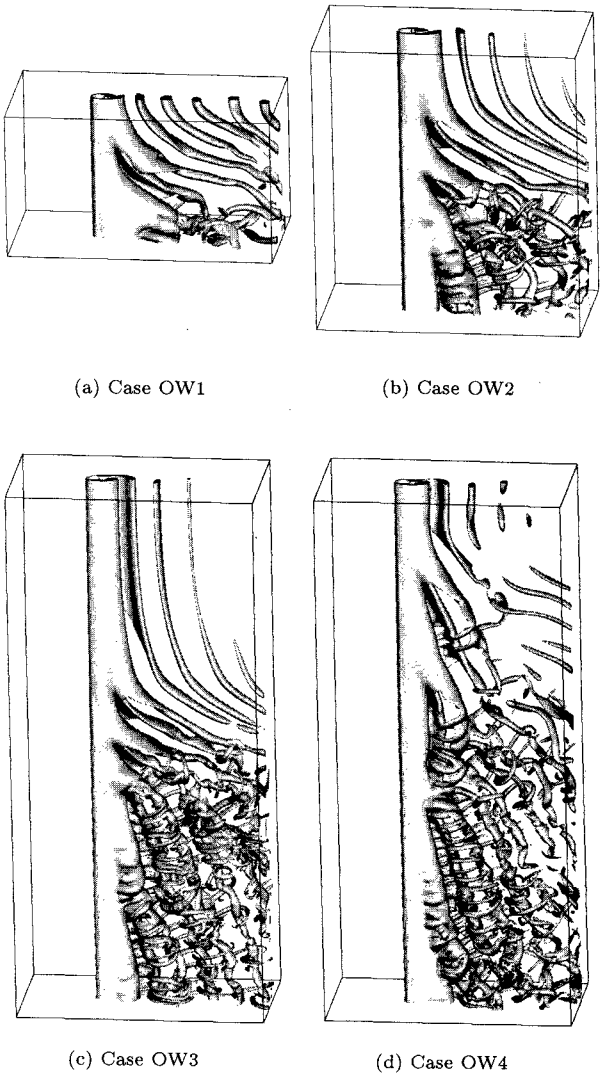

(a) Case OW1 (b) Case OW2

(c) Case OW3 (d) Case OW4

Figure 2: Perspective views showing isosurfaces of the vorticity modulus divided locally by the inlet streamwise velocity.

the oblique vortex shedding. In particular, it can be observed that the formation of Kármán vortices is triggered preferentially in the high-speed region of the flow and is propagated towards positive y-coordinates. From this view, the angle of the vortex shedding appears to be conditioned by the characteristic speed of this vortex shedding propagation in y-direction. This driving of the vortex dynamics near $y \approx -L_y/2$ suggests a strong receptivity of the flow dynamics in this region, a property that could be interesting in the context of flow control.

Further downstream, in regions where the shear is significant ($-L'_y/2 < y < L'_y/2$), the obliqueness of the wake structures is increased by a simple convective mechanism. Due to the high value of the shear parameter β, the obliqueness of large-scale vortices is very pronounced in the shear region for the cases OW1, OW2 and OW3. Further downstream, these structures twist in an alternatively clockwise and counter-clockwise way. In the simulation OW4 for which the parameter β is more moderate, the oblique character of the vortex shedding is logically less pronounced in the shear region. However, animations show clearly a continual re-orientation of the Kármán vortices as they are convected downstream. In an idealized constant-shear flow

$U(y) = U_c(1 - \beta y/D)$, it is easy to show that the angle $\theta(t)$ between a Lagrangian line and the shear axis follows the temporal law $\theta(t) = \text{atan}\left(\tan\theta_0 + \frac{U_c\beta}{D}t\right)$ where θ_0 is the initial angle at $t = 0$. Following this very simplified view, it is natural to expect that the downstream transport of Kármán vortices in the shear region tends to increase their obliqueness until they are aligned on the longitudinal direction. This second mechanism of slantwise vortex formation is illustrated on figure 4 where the main directions of some Kármán vortices are approximately indicated by lines. On this figure, the difference between cases OW3 and OW4 is very clear. For the OW3 case, in the high-speed region of the flow (locally free of shear), the Kármán structures form obliquely and keep their initial directions further downstream. In contrast, the obliqueness of Kármán vortices continuously increases with x for the OW4 case, as it can be expected from convection effects. Naturally, this re-orientation mechanism by transport is more efficient in regions highly sheared, as it can be observed in the four cases (see figure 2).

Due to high values of the shear β and its vertical extension L'_y considered here, the occurrence of Kármán vortices crossing the complete computational domain in y-direction is never observed. The more extended oblique vortices are found in the cases OW3 and OW4, in high-speed region as well as in low-speed region of the flow.

Analysis of 3D motions

Before describing the spatial organization of 3D motions, it is useful to clarify the nature of the four flow configurations considered here. As already stressed in a previous section, it is possible to define a local Reynolds number $Re_l(y) = U(y)D/\nu$ associated to the inflow velocity profile. In the four cases considered here, Re_l covers the same range $Re_l(y) \in [Re_1, Re_2]$ with $Re_1 = U_1D/\nu = 100$ to $Re_2 = U_2D/\nu = 300$. In a conventional wake behind a cylinder ($U_1 = U_2$), the Reynolds number dependence of the flow dynamics is considerable in the range $Re \in [100, 300]$. Schematically, three typical flow regimes are currently found. When $100 < Re < 190$, a purely two-dimensional vortex shedding occurs. Above this critical value, three-dimensional motions appears. In the transition regime $190 < Re < 260$, the 3D instability leads to the formation of longitudinal vortices spaced in y-direction at a typical wavelength of around $3 - 4$ diameters. These structures are related to an instability called mode A. From $Re \approx 230$, this mode is gradually replaced by the mode B instability which leads to the appearance of a second class of 3D structures of finer scale. In the last range $260 < Re < 300$ covered in present flow configuration, mode B becomes dominant, the main topological change of the wake being related to the wavelength selection of longitudinal structures (stretched between Kármán vortices) which are spaced by about only one diameter.

If the present flow configuration is idealized as a set of independent 2D wakes (by neglecting vertical motions, especially the upward/downward currents in front of/behind the cylinder respectively) of decreasing Reynolds number as y increases, three flow regimes are expected to coexist in the same computational domain. The observation of each visualization presented on figure 2 shows that this somewhat over-simplified view is basically recovered for cases OW2 and OW3, especially concerning the two-dimensional behaviour of the flow in the low-speed region and the appearance of the mode B instability in the high region. The transition regime is more delicate to identify for the case OW2, while being indistinguishable for the other cases. For the flows OW1 and OW2, the effects of free-slip walls do not allow an easy identification of local flow regimes. However, in all flow configurations, strong secondary vortices are created between the distorted Kármán vortices in the high-speed region of the flow. Note however that for the case OW1, the 3D organization of the flow near the lower free-slip wall does not allow us to identify formally a vortex shedding process. Finally, it is interesting to observe that in region where Kármán vortices are strongly inclined (cases OW1, OW2, OW3), a very unusual vortical topology is obtained where secondary vortices are mainly oriented in the vertical direction contrary to the conventional case where equivalent structures are stretched in the streamwise direction.

Cellular pattern of vortex shedding

Even if an adjustment of the vortex shedding frequency on the local upstream velocity $U(y)$ can be expected, the preservation of the coherence of the motion in y-direction prevents this process to be purely local. Schematically, the coherence of the vortices tends to maintain a phase relation in y-direction over a significant physical length. The critical value of this length corresponds to the size of a cell where, by definition, the vortex shedding frequency should be constant. The formation of cells in the vortex shedding behind a body in a shear flow was already noted in previous studies (Maull and Young, 1973; Stansby, 1976; Tavoularis et al., 1987, Woo et al. 1989; Mukhopadhyay et al., 2002). A simple theoretical model was proposed by Noack et al. (1991) for this phenomenon at low Reynolds number ($100 < Re < 160$). For the present results, a simple observation of the animations does not allow us to identify unambiguously the cell formation mechanisms. For the case at moderate shear (OW4), oblique Kármán-like vortices of moderate span can be identified, but it is delicate to locate formally the corresponding cells. Despite this difficulty, it is interesting to observe that periodically, a phase breaking occurs in a dislocation process in agreement with previous observations. In present results, dislocations can be clearly observed on animations through the identification of vortices which are torn by the main flow. For the case OW1, only one cell can be clearly identified, the 3D motions near the lower free-slip wall being not organized enough to allow us to distinguish any vortex shedding process. For the cases OW2 et OW3, two cells can be easily identified outside the shear region. These two cells seem to synchronize the flow in the central region $-L'_y/2 < y < L'_y/2$ where the occurrence of highly 3D motions prevents to identify clearly the presence of other cells.

Frequency analysis

A more rigorous identification of the number and size of cells needs to consider quantitatively the spatial repartition (along the y-direction) of the main frequencies governing the flow dynamics. For this purpose, a set of temporal data was stored for several x and y locations. The length of the time series used is $T = 114D/U_c$. The frequencies f associated to each time series was obtained by means of Fourier analysis based on conventional FFT. Here, we present only data corresponding to the streamwise position $x - x_{cyl} = 2D$ in the symmetric plane $z = 0$. In order to show the vertical variability of the flow, typical time series and their associated spectra (vs. the dimensionless frequency fD/U_c) are presented by covering the full extent of the computational

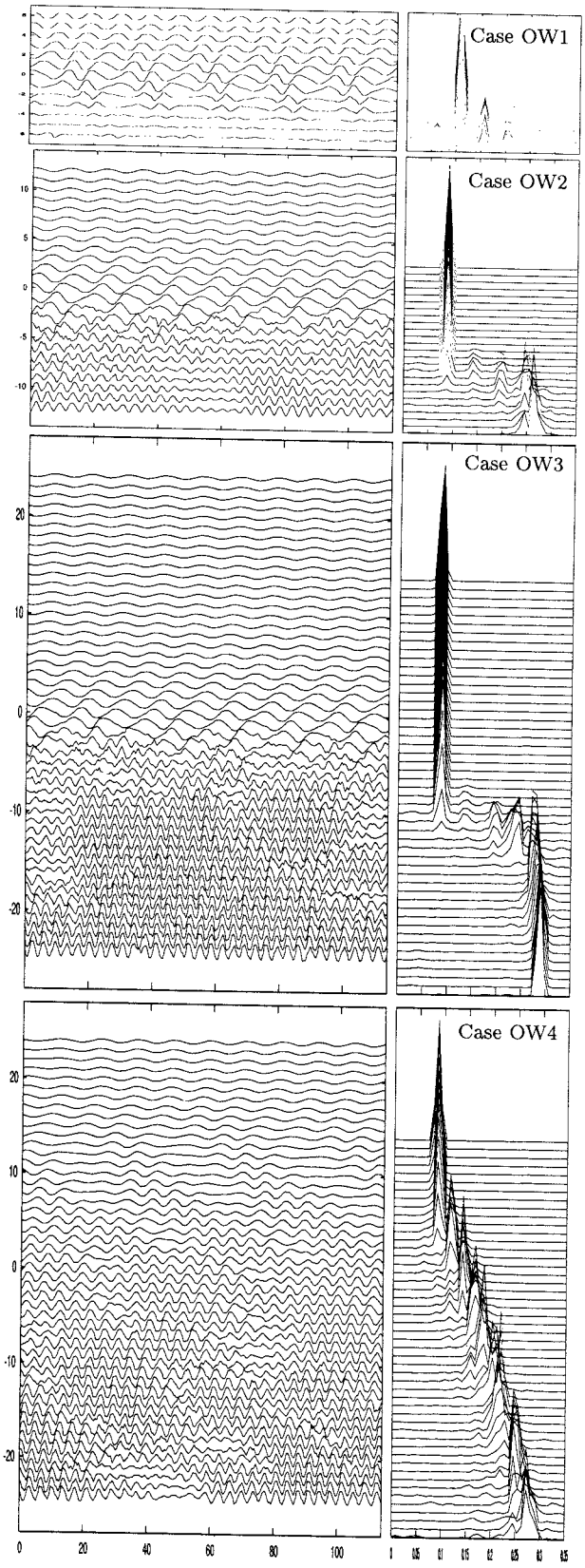

Figure 3: Vertical variation from $y = -L_y/2$ to $y = L_y/2$ of time series (left) and their frequency spectra of transverse velocity (right) at $x - x_{cyl} = 1D$ and $z = 0$. The power spectra density vertical axe is on an arbitrary scale. Curve for each vertical location (where y/D takes an integer value) is plotted with a successive offset.

domain in y-direction. The four cases OW1, OW2, OW3 and OW4 are presented on figure 3.

Let us first consider the main frequencies associated to the locally constant high- and low-speed flows of velocity U_1 and U_2 respectively. These both frequencies can be deduced by the examination of spectra which admit two marked peaks near the locations $y = \pm L_y/2$. In order to establish a link between this values and the one corresponding to a conventional wake, it is convenient to define the two local Strouhal numbers $St_1 = fD/U_1$ and $St_2 = fD/U_2$ where f is the frequency understudy. For cases OW2, OW3 and OW4, a similar value is found in the low-speed region of the flow with $St_1 \approx 0.16$. This value is close to the one obtained for a conventional wake at $Re = 100$ (Williamson, 1996). For the case OW1, the value given by spectra peaks near $y \approx L_y/2$ is significantly increased with $St_1 = 0.22$. This increase of the vortex shedding frequency seems to be an effect of the upper free-slip wall which is very close to the shear region due to the moderate extension of the computational domain in y-direction. In the high-speed region, the presence of the lower free-slip wall influences more strongly the frequency selection of the vortex shedding. Hence, we obtain $St_2 \approx (0.17, 0.19, 0.18)$ for cases (OW2,OW3,OW4) respectively. These values are lower than for a conventional wake at $Re = 300$ where $St = 0.2$ is a well accepted value. Note that the decrease of St_2 is more pronounced when L'_y is close to L_y.

The examination of the vertical variation of spectra presented on figure 3 shows that the main frequency selection is strongly affected by the shear parameter β and by the ratio L'_y/L_y. For the case OW1, several peaks are clearly visible. Super- and sub-harmonic frequencies can be identified at the same y-location, especially in the high-speed region where we cannot observe a clear dominant frequency, confirming the idea that the vortex shedding is strongly destructured. For the other cases OW2, OW3 and OW4, at each y-location, the domination of a single frequency is more marked, suggesting the occurrence of a regular vortex shedding. An interesting point is that the main frequency varies by jump from a y-location to another. This behaviour can be related to the vertical coherence of vortex shedding which is organized, as already discussed previously, in cells distributed along the cylinder.

In order to better analyse the vortex shedding frequency selection, let us consider more specifically the cases OW3 et OW4. Figure 4 presents views comparing visualizations and y-locations of main frequencies. In addition, an idealized frequency profile is plotted. This reference frequency, local by nature, is estimated by

$$f_i(y) = \frac{U(y)\cos\theta}{D}\left(0.212 - \frac{4.5\nu}{U(y)D}\right) \qquad (3)$$

This relation is simply a local adaptation of the Roshko's empirical law $St = 0.212 - 4.5/Re$ including the correction by the cosine of the angle formed by the oblique vortices just behind the cylinder. In the context of a conventional cylinder wake, this correction was demonstrated to be useful to predict accurately the reduction of the shedding frequency when oblique shedding appears (Williamson, 1996; Mittal, 2001). Here, we crudely approximate the angle θ by zero in the slowest region of the flow ($Re \approx 100$) where the vortex shedding is locally parallel, whereas in the rest of the domain, we affect to this angle a constant value with $\theta \approx 15$ and $\theta \approx 20$ for the cases OW3 and OW4 respectively, in agreement with the visual mean inclination of the vortices observed on animations just behind the cylinder. The

comparison between the idealized frequency profile and the frequencies measured emphasizes very well the occurrence of synchronization mechanisms preserving the vertical coherence of the flow. Outside of the shear region, for both cases OW3 and OW4, a quite good agreement is obtained between the measured frequencies and the idealized ones. In contrast, the selection of the main frequency can strongly deviate from its idealized estimation in the sheared zone, especially for the case OB3 in the low frequency range. For this case, the frequency selection in the shear regions seems to be mainly conditioned by the vortex shedding in the low-speed side of the flow without any local adjustment on the mean velocity $U(y)$. Near $y = -L'_y/2$, the main frequency suddenly returns near its idealized estimation through a considerable jump (see figure 4). For lower y, about three plateau values can be observed, suggesting again a cellular structure of the vortex shedding in this region of the flow. Similarly, for the case OW4, about nine cells can be identified, but it should be recognized that in the high-speed part of the flow, due to the highly 3D motions, the location of the cell boundaries is not possible to determine unambiguously. Despite this reservation, the variation by jump (preserving the y-coherence of the flow in a significant y-extension) of the main frequency in order to maintain a local Strouhal number closed to the conventional cylinder wake is well recovered for OW4. Moreover, the large number of cells noticed is consistent with the observation that this case leads to numerous vortex dislocations, as clearly shown by the animations.

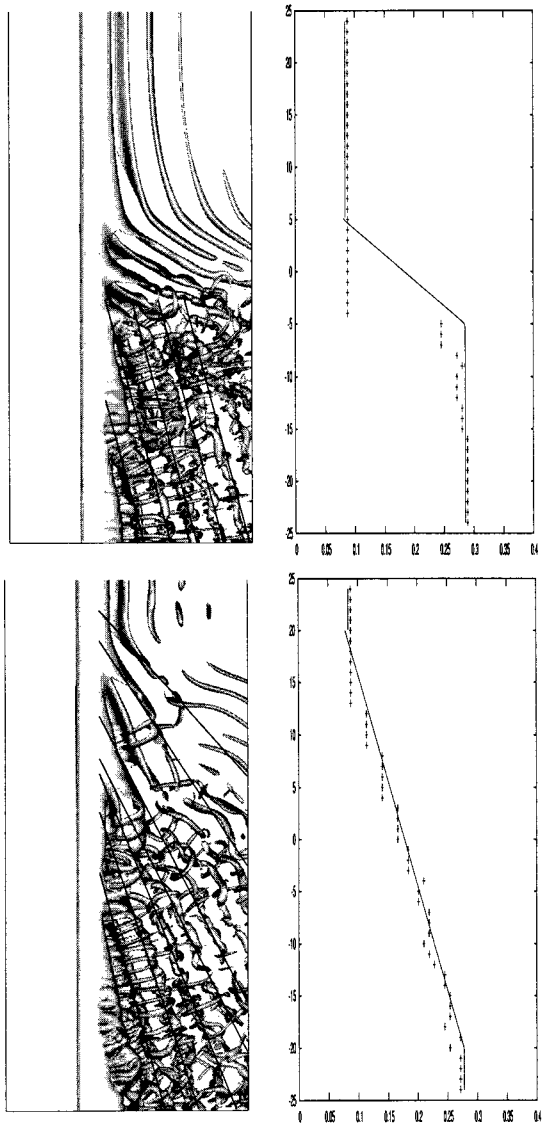

(a) Side views showing an isosurface of the vorticity modulus divided locally by the inlet streamwise velocity

(b) Vertical variation of the main frequencies corresponding to spectra maximums presented on figure 3

Figure 4: Comparison of instantaneous visualizations (a) and main frequency profiles (b).

ACKNOWLEDGMENTS

The present calculations and visualizations were carried out at the IDRIS, the computational centre of the CNRS. We are grateful to Thierry Goldmann (IDRIS) for its precious help for the generation of graphical animations. Francis Boissonneau, Jean-François Largeau and Valérie Lefeuvre are also gratefully acknowledged. This study was partially supported by the CNRS.

REFERENCES

D. Goldstein, R. Handler, and L. Sirovich., 1993, Modeling a no-slip boundary condition with an external force field. *J. Comp. Phys.*, **105**:354–366.

D. Heitz., 1999, *Etude expérimentale du sillage d'un barreau cylindrique se développant dans une couche de mélange plane turbulente.* PhD thesis, Université de Poitiers.

E. Lamballais and J. Silvestrini., 2002, Direct numerical simulation of interactions between a mixing layer and a wake around a cylinder. *J. Turbulence*, 3:028.

S. Lardeau, E. Lamballais, and J.P. Bonnet., 2002, Direct numerical simulation of a jet controlled by fluid injection. *J. Turbulence*, 3:002.

D. J. Maull and R. A. Young., 1973, Vortex shedding from bluff bodies in a shear flow. *J. Fluid Mech.*, **60**:401–409.

S. Mittal., 2001, Computation of three-dimensional flows past circular cylinder of low aspect ratio. *Phys. Fluids*, **13**(1):177–191.

A. Mukhopadhyay, P. Venugopal, and S. Vanka., 2002, Oblique vortex shedding from a circular cylinder in linear shear flow. *Computers and FLuids*, **31**:1–24.

B. R. Noack, F. Ohle, and H. Eckelmann., 1991, On cell formation in vortex streets. *J. Fluid Mech.*, **227**:293–308.

J.H. Silvestrini and E. Lamballais., 2002, Direct numerical simulation of wakes with virtual cylinders. *Int. J. Comp. Fluid Dynamics*, **16**(4):305–314.

P. K. Stansby., 1976, The locking-on of vortex shedding due to the cross-stream vibration of circular cylinders in uniform and shear flows. *J. Fluid Mech.*, **74**:641–665.

S. Tavoularis, H. Stapountzis, and U. Karnik., 1987, Vortex shedding from bluff cylinders in strongly sheared turbulent streams. *J. of Wind Eng. and Ind. Aerodynamics*, **26**:165–178.

C.H.K. Williamson., 1996, Vortex dynamics in the cylinder wake. *Ann. Rev. Fluid Mech.*, **28**:477–539.

H. G. C. Woo, J. E. Cermak, and J. A. Peterka., 1989, Secondary flows and vortex formation around a circular cylinder in constant-shear flow. *J. Fluid Mech.*, **204**:523–542.